Magnetic adatoms as memory bits: A quantum master equation analysis

Christian Karlewski,[1,2,*] Michael Marthaler,[1] Tobias Märkl,[3]
Timofey Balashov,[3] Wulf Wulfhekel,[2,3] and Gerd Schön[1,2]

[1]*Institut für Theoretische Festkörperphysik, Karlsruhe Institute of Technology, D-76131 Karlsruhe, Germany*
[2]*Institute of Nanotechnology, Karlsruhe Institute of Technology, D-76344 Eggenstein-Leopoldshafen, Germany*
[3]*Physikalisches Institut, Karlsruhe Institute of Technology, D-76131 Karlsruhe, Germany*
(Dated: May 11, 2015)

Due to underlying symmetries the ground states of magnetic adatoms may be highly stable, which opens perspectives for application as single-atom memory. A specific example is a single holmium atom (with $J = 8$) on a platinum (111) surface for which exceptionally long lifetimes were observed in recent scanning tunneling microscopy studies. For control and read-out the atom must be coupled to electronic contacts. Hence the spin dynamics of the system is governed by a quantum master equation. Our analysis shows that in general it cannot be reduced to a classical master equation in the basis of the unperturbed crystal-field Hamiltonian. Rather, depending on parameters and control fields, "environment induced superselection" principles choose the appropriate set of basis states, which in turn determines the specific relaxation channels and lifetimes. Our simulations suggest that in ideal situations the lifetimes should be even longer than observed in the experiment. We, therefore, investigate the influence of various perturbations. We also study the initialization process of the state of the Ho atom by applied voltage pulses and conclude that fast, high fidelity preparation, on a 100 ns timescale, should be possible.

PACS numbers: 72.25.-b, 05.30.-d, 03.65.Yz

I. INTRODUCTION

An ultimate boundary of miniaturization of information technology is reached when single atoms are used as memory bits. In this respect the experiment of Miyamachi *et al.* [1] with a single Ho atom positioned on a Pt(111) surface (as depicted in Fig. 1) represent an important milestone, promising lifetimes of several minutes for the two degenerate magnetic ground states. For the crystal-field Hamiltonian with parameters as determined in Ref. [1], the two ground states of the Ho atom have $\langle J_z \rangle \approx \pm 8$ pointing into or out of the metal surface. The long lifetimes result from a combination of symmetries and specific properties of the system [1]. They are many orders of magnitude longer than those measured for single Co/Fe atoms on Pt(111) [2, 3] or other magnetic adatoms on a metallic surface [4]. A related giant magnetic anisotropy of single adatoms had been observed earlier for Co atoms on Pt(111) [5]. We should mention that in another recent work with Ho on Pt(111), Donati *et al.* [6] arrived at different crystal-field parameters, leading to ground states with $\langle J_z \rangle \approx \pm 6$ and much shorter lifetimes.

In this paper we develop the theory how to treat magnetic adatoms on metallic surfaces which – for read-out and control – are coupled to electronic reservoirs formed by the metal substrate and a spin-polarized STM tip. The description of this dissipative system is based on a quantum master equation for the reduced density matrix for the angular momentum states, which accounts for the
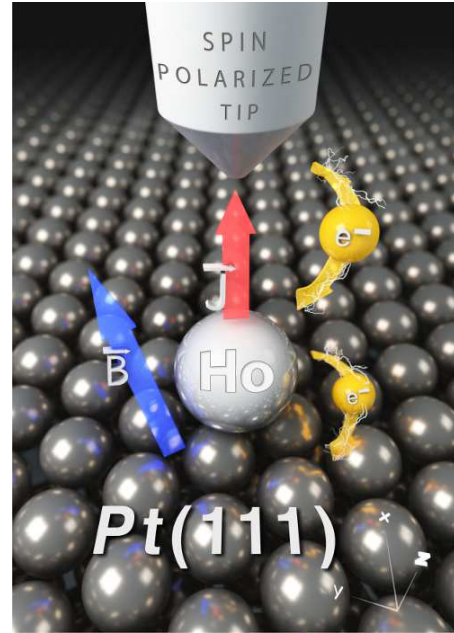

FIG. 1. Setting of the experiment in Ref. [1]: The magnetic state of an holmium atom on a Pt(111) surface is studied by a scanning tunneling microscope with a spin-polarized tip.

influence of the electronic contacts and the applied voltage. For low voltages the description reduces to a rate equation in the eigenbasis of the unperturbed crystal-field Hamiltonian, which are specific superpositions of angular momentum states. However, for larger voltages the coherence of these superposition states is destroyed, and the relevant states are the steady-state eigenstates of the full dissipative quantum master equation. This is an

example for what has been called "environment-induced superselection" (or short "einselection") principle [7, 8]. In the considered system the choice of the appropriate basis depends strongly on the voltage. It strongly influences the relaxation channels and times. Switching the voltages also allows initializing the systems in a specific ground state, which is needed when using the system as memory.

As a specific example we analyze Ho on Pt(111) with crystal-field Hamiltonian as determined in Ref. [1], but we also compare with the situation obtained for the parameters of Ref. [6]. The quantitative comparison with the experiments requires assumptions about a number of further parameters, which we explore in the latter part of this paper in some detail. For the comparison we also present experimental data which resolve, beyond what has been reported in Ref. [1], the lifetimes for each one of the low-energy states.

II. THE MODEL

A. The crystal-field Hamiltonian and eigenstates

We investigate the dynamics of a magnetic adatom placed on a high-symmetry position on a metal surface in a situation where the symmetry stabilizes the degenerate ground states against the dominant perturbations. Such a situation is realized for Ho on Pt(111), which we consider as a specific example, but our analysis and conclusions can easily be generalized to other magnetic adatoms. Ho adatoms on a Pt(111) surface have been investigated experimentally in Refs. [1, 6, 9]. The Ho atom has strong spin-orbit coupling, therefore the total angular momentum is a good quantum number with $J = 8$, leading to 17 states in the multiplet to be studied. A single adatom on a crystal structure with trigonal symmetry can be described by a crystal-field Hamiltonian adjusted to the symmetries [10, 11],

$$H_{CF} = \sum_{\substack{n=2,4,6 \\ m=0,3,6 \\ m \leq n}} B_n^m O_n^m \tag{1}$$
$$= B_2^0 \cdot 3\, J_z^2 + B_4^0 \cdot 35\, J_z^4$$
$$+ B_4^3 \cdot \frac{1}{4} \left[J_z, (J_+^3 + J_-^3) \right]_+ + \cdots .$$

Here O_n^m are the Stevens operators expressed in powers of J_z, J_+ and J_- angular momentum operators of the Ho atom [12]. Due to the trigonal symmetry the operators J_+ and J_- appear in powers of multiples of three. Above, the first three terms are shown explicitly (with $[\cdot, \cdot]_+$ denoting the anti-commutator), further ones are listed in the Appendix. The coefficients B_n^m are crystal-field parameters, which in Ref. [1] were determined from *ab-initio* calculations and compared with experiment. For Ho and many other magnetic adatom

systems the leading term is $\propto J_z^2$ with a negative coefficient $B_2^0 < 0$. The difference in the conclusions reached in Refs. [1] and [6] arise from different values of the parameter B_4^0. We first proceed using the values of Ref. [1] but we will comment of the situation of Ref. [6] in section V E.

The eigenstates of the crystal-field Hamiltonian H_{CF} can be divided into three families of states, $|\psi_m^+\rangle$, $|\psi_m^-\rangle$, and $|\psi_m^0\rangle$. Each one of these states is a superposition of different J_z eigenstates with magnetic quantum numbers differing by multiples of 3. The lower index m of each state, with $-8 \leq m \leq 8$, denotes the dominantly contributing J_z eigenstate. In Fig. 2 we plot the eigenenergies versus the expectation value $\langle J_z \rangle$. They are marked by circles, squares and triangles for the three families $+, -, 0$. Since the dominant contribution to the eigenenergies arises from the first term $\propto -J_z^2$ the energies lie approximately on an inverted parabola. Note that by plotting the energy versus $\langle J_z \rangle$ we can also represent arbitrary superposition states of the aforementioned basis states, which is useful for the following discussions.

The two degenerate ground states of the system $|\psi_8^+\rangle$ and $|\psi_{-8}^-\rangle$, with differing angular moment pointing into or out of the surface, belong to two different families (+ and −). The same applies for the first excited states $|\psi_7^+\rangle$ and $|\psi_{-7}^-\rangle$, as well as for various higher ones. These states are superposition of non-degenerate J_z-eigenstates. In contrast, the states $|\psi_{6s}^0\rangle$ and $|\psi_{6a}^0\rangle$, belonging to the 0−family, are superpositions made up of degenerate J_z-eigenstates, coupled by the operators O_4^3, O_6^3 and O_6^6. They naturally split into symmetric and antisymmetric (s,a) combinations, both with vanishing $\langle J_z \rangle$, and are marked accordingly in Fig. 2 a). The same applies for $|\psi_{3s}^0\rangle$ and $|\psi_{3a}^0\rangle$.
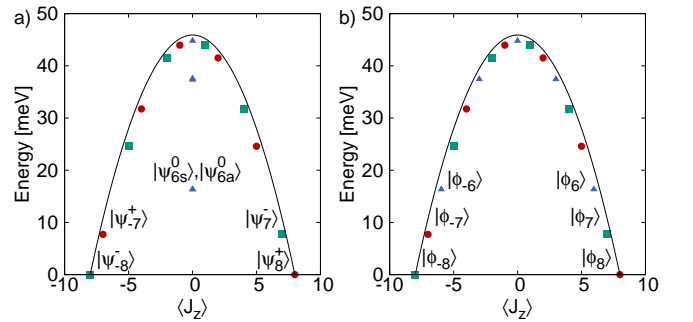

FIG. 2. a) Energies of the eigenstates of the Hamiltonian H_{CF} plotted versus the expectation value $\langle J_z \rangle$. b) Energy expectation values of the steady states $|\phi_m\rangle$ of the quantum master equations for strong dissipation due to an applied voltage of $U = 7.3\,\text{mV}$. The labels refer to the dominantly contributing J_z-eigenstates.

B. Spin-dependent electron scattering

For control and read-out of the magnetic state the Ho adatom is coupled to a spin-polarized STM tip. The electronic reservoirs influence the dynamics of the system by the scattering of electrons in the electrodes from the atom and by the tunneling of electrons between tip and bulk substrate via the atom (see Fig. 1). Accordingly the total Hamiltonian consists of three parts, $H = H_S + H_{Res} + H_C$, describing the system, the electron reservoirs in the bulk substrate and tip of the STM, and the coupling terms,

$$H_S = H_{CF} + g_J \mu_B \vec{B} \cdot \vec{J}, \tag{2}$$

$$H_{Res} = \sum_{\substack{\alpha = T, B \\ \sigma = \uparrow, \downarrow; k}} (\varepsilon_{k\sigma}^{\alpha} + eU^{\alpha})\, c_{k\sigma}^{\alpha\dagger} c_{k\sigma}^{\alpha}, \tag{3}$$

$$H_C = \sum_{\substack{\alpha, \alpha' = T, B \\ kk'}} t_{kk'}^{\alpha\alpha'} \left[J_+ c_{k\downarrow}^{\alpha\dagger} c_{k'\uparrow}^{\alpha'} + J_- c_{k\uparrow}^{\alpha\dagger} c_{k'\downarrow}^{\alpha'} \right.$$
$$\left. + J_z \left(c_{k\uparrow}^{\alpha\dagger} c_{k'\uparrow}^{\alpha'} - c_{k\downarrow}^{\alpha\dagger} c_{k'\downarrow}^{\alpha'} \right) \right]. \tag{4}$$

In (2) we added the contribution due to an applied or stray magnetic field $\vec{B}$, with g_J being the Landé-factor, μ_B the Bohr magneton. The bath electron, with creation (annihilation) operators $c_{k\sigma}^{\alpha\dagger}$ ($c_{k\sigma}^{\alpha}$), have energies $\varepsilon_{k\sigma}^{\alpha}$ where α can be T or B for the spin-polarized tip or the bulk substrate. We also account for the voltage of the baths U^{α}. In (4) we concentrate on the interaction of the spins of the electrons with the angular momentum $\vec{J}$ of the atom, which leads to scattering and tunneling processes, with or without spin flip, with amplitudes $t_{kk'}^{\alpha\alpha'}$ described by the three terms in H_C. For $\alpha = \alpha' = B$ these terms describe the scattering of a bulk electron, while for $\alpha \neq \alpha'$ they describe tunneling between the tip and the bulk via the Ho atom. Other couplings of the total angular momentum to, e.g., phonons or the radiation field and the resulting dissipative effects are not considered explicitly in this work, but will be accounted for in a qualitative way in section V C. We further have to keep in mind that the measured current between tip and substrate is also caused by further spin-independent coupling terms.

The eigenstates $|\psi_m^{\pm}\rangle$ of the crystal-field Hamiltonian have the property that two eigenstates with the same energy but from different families have vanishing matrix elements $\langle \psi_m^{\sigma} | J_\nu | \psi_{-m}^{-\sigma} \rangle = 0$ for $\nu \in \{+, -, z\}$, $\sigma = \pm$ and all m. It is a consequence of two properties of the system: First, the C_{3v} symmetry of the adsorption site, which leads to the Stevens-operators introduced above with operators J_+ and J_- appearing in powers of multiples of three. Second, the time-reversal symmetry for $\vec{B} = 0$ with the following properties of the time reversal operator $\mathcal{T}$ (see Ref. [1]),

$$\mathcal{T}^2 = 1, \qquad \langle \chi | \phi \rangle = \langle \mathcal{T}\phi | \mathcal{T}\chi \rangle,$$
$$\mathcal{T} J_\nu = -J_\nu \mathcal{T}, \quad \mathcal{T} |\psi_m^{\sigma}\rangle = |\psi_{-m}^{-\sigma}\rangle. \tag{5}$$

From these relations we find $\langle \psi_m^{\sigma} | J_\nu | \psi_{-m}^{-\sigma} \rangle = 0$ since

$$\langle \psi_m^{\sigma} | J_\nu | \psi_{-m}^{-\sigma} \rangle = \langle \mathcal{T}\psi_m^{\sigma} | \mathcal{T} J_\nu \psi_{-m}^{-\sigma} \rangle^* = -\langle \psi_{-m}^{-\sigma} | J_\nu \mathcal{T} \psi_{-m}^{-\sigma} \rangle^*$$
$$= -\langle \psi_{-m}^{-\sigma} | J_\nu | \psi_m^{\sigma} \rangle^* = -\langle \psi_m^{\sigma} | J_\nu | \psi_{-m}^{-\sigma} \rangle. \tag{6}$$

Thus, a transition between the two ground states with $m = \pm 8$ (and similar $m = \pm 7$) cannot be induced by a single electron scattering, which is crucial for their observed long lifetimes [1].

On the other hand, at non-zero temperature $T \neq 0$ and under the influence of an applied voltage U, scattering and tunneling of electrons may lead to transitions to exited states and eventually to transitions between the two ground states. Additionally, time-reversal symmetry breaking terms in the Hamiltonian, such as a magnetic field, give rise to direct transitions between the ground states. These effects lead to a finite relaxation time T_1, which has been probed in the experiment and is the first and central quantity to be studied in this paper. In a later section we will also investigate the decoherence time T_2, i.e., the time scale for the decay of a coherent superposition of the two ground states.

The temperature in the experiments [1] was as low as $0.7\,\mathrm{K}$ (i.e., $k_B T \approx 0.060\,\mathrm{meV}$), whereas the typical system energy, i.e. the first excitation energy is $7.7\,\mathrm{meV}$. Thus, the system is clearly in the quantum regime.

III. QUANTUM MASTER EQUATION

A. Damping due to electron scattering and tunneling

The description of the system in the quantum regime under the influence of the electronic reservoirs requires solving the reduced quantum master equation appropriate for open quantum systems [13, 14],

$$\dot{\rho}(t) = i\left[\rho(t), H_S\right] + \int_{t_0}^{t} dt'\, \Sigma(t - t')\rho(t'). \tag{7}$$

Here and below we set $\hbar = 1$. The influence of the two electronic reservoirs enters in the dissipative kernel $\Sigma(t - t')$. We assume it to be of a Lindblad form and use a Born-Markov approximation. In the interaction picture the quantum master equation for the 17 states of the system then reduces to

$$\dot{\rho}_I = -\sum_{\substack{\nu, \nu' = +, -, z \\ \alpha, \alpha' = T, B}} \int_0^{\infty} dt' \tag{8}$$

$$\left\{ \left[J_\nu(t) J_{\nu'}(t')\rho_I(t) - J_{\nu'}(t')\rho_I(t) J_\nu(t) \right] C_{\nu\nu'}^{\alpha\alpha'}(t - t') \right.$$

$$\left. + \left[\rho_I(t) J_{\nu'}(t') J_\nu(t) - J_\nu(t)\rho_I(t) J_{\nu'}(t') \right] C_{\nu\nu'}^{\alpha\alpha'}(t' - t) \right\},$$

with the dissipative kernel expressed by the correlation functions

$$C_{\nu\nu'}^{\alpha\alpha'}(t) = \sum_{k,k'} |t_{kk'}^{\alpha\alpha'}|^2 \langle s_{kk'\nu}^{\alpha\alpha'}(t) s_{k'k\nu'}^{\alpha'\alpha}(0) \rangle \quad (9)$$

with

$$s_{kk'-}^{\alpha\alpha'} = c_{k\downarrow}^{\alpha\dagger} c_{k'\uparrow}^{\alpha'}, \; s_{kk'+}^{\alpha\alpha'} = c_{k\uparrow}^{\alpha\dagger} c_{k'\downarrow}^{\alpha'},$$
$$s_{kk'z}^{\alpha\alpha'} = c_{k\uparrow}^{\alpha\dagger} c_{k'\uparrow}^{\alpha'} - c_{k\downarrow}^{\alpha\dagger} c_{k'\downarrow}^{\alpha'}. \quad (10)$$

Assuming $t_{kk'}^{\alpha\alpha'} \approx t^{\alpha\alpha'}$ and introducing the spin-dependent electron densities of states at the Fermi-edge N_σ^α with $\sigma = \uparrow, \downarrow$ we obtain the Fourier transformed of the correlation functions,

$$\tilde{C}_{+-}^{\alpha\alpha'}(\Lambda_{nm}) = |t^{\alpha\alpha'}|^2 N_\uparrow^\alpha N_\downarrow^{\alpha'} \zeta(\Lambda_{nm} + e(U^\alpha - U^{\alpha'}))$$
$$\tilde{C}_{-+}^{\alpha\alpha'}(\Lambda_{nm}) = |t^{\alpha\alpha'}|^2 N_\downarrow^\alpha N_\uparrow^{\alpha'} \zeta(\Lambda_{nm} + e(U^\alpha - U^{\alpha'}))$$
$$\tilde{C}_{zz}^{\alpha\alpha'}(\Lambda_{nm}) = |t^{\alpha\alpha'}|^2 \left(N_\uparrow^\alpha N_\uparrow^{\alpha'} + N_\downarrow^\alpha N_\downarrow^{\alpha'} \right)$$
$$\times \zeta(\Lambda_{nm} + e(U^\alpha - U^{\alpha'})). \quad (11)$$

They are evaluated at the energy differences of the atomic system, $\Lambda_{nm} = E_m - E_n$ shifted by the applied voltages. Here we introduced

$$\zeta(\omega) = \int f(E)\left[1 - f(E - \omega)\right] dE = \frac{\omega}{\exp[\omega/(k_B T)] - 1},$$

where $f(E) = [e^{E/(k_B T)} + 1]^{-1}$ is the Fermi function.

As usual in the context of the tunneling magneto-resistance we define the tip polarization $\eta = (P_\uparrow - P_\downarrow)/(P_\uparrow + P_\downarrow) \in [-1, 1]$, where the spin up/down populations are proportional to the densities of states $P_{\uparrow/\downarrow} \propto N_{\uparrow/\downarrow}^T = N^T \cdot \frac{1}{2}(1 \pm \eta)$. The bulk electrode is assumed to be non-polarized, hence $N_{\uparrow/\downarrow}^B = N^B$. The remaining parameters, apart from the polarization η, can be lumped in the coefficients

$$c_{\alpha\alpha'} = \frac{1}{2} |t^{\alpha\alpha'}|^2 N^\alpha N^{\alpha'}.$$

In the following discussions of the relaxation processes we will concentrate mostly on applied voltages $U = U^T - U^B$ of the order of or exceeding $3\,\text{mV}$. In this case the effect of tunneling electrons is stronger than that of scattering electrons in the bulk electrode, which in turn is assumed to be stronger than the scattering in the tip. We therefore set $c_{TT} = 0$ in most of the paper. Furthermore, we start with $c_{BB} = 0$, but we will analyze the influence of bulk electrons scattering in section V A. Also for the calculation of the dephasing time T_2 for zero current in section VI the scattering terms need to be taken into account.

B. The proper basis states and environment-induced superselection

If the system behaves sufficiently classically, it is possible to reduce the quantum master equation to rate equa-
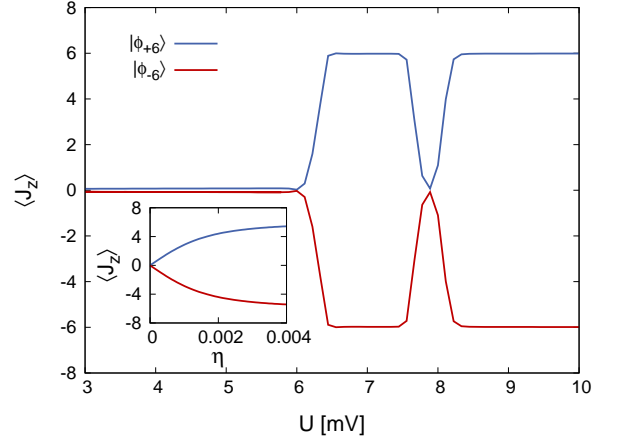

FIG. 3. Expectation value $\langle J_z \rangle$ versus the voltage U for a tip polarization $\eta = -0.15$, and in the inset versus the polarization η for $U = 7.3\,\text{mV}$. The other parameters are $B_z = 10^{-8}\,\text{T}$ and $c_{TB} = 3.41 \cdot 10^6 (\text{meV s})^{-1}$.

tions for the populations P_i of the different states

$$\frac{dP_i}{dt} = \sum_j \left(\Gamma_{ji} P_j - \Gamma_{ij} P_i \right), \quad (12)$$

with Γ_{ji} describing the transition rates between the different states. Such a reduction is possible if the coherences, i.e., the off-diagonal components of the density matrix decay much faster than non-equilibrium populations. The question remains, what is the appropriate basis to decouple the coherences and populations. One frequently used option for this basis are the eigenstates of H_{CF}. It is the appropriate choice if the influence of the baths is weak, and the eigenstates are only little affected by their presence. This choice and the resulting reduction to rate equations has been used, e.g., in Refs.[15–19] and allows an easy interpretation of transition channels.

In general, the quantum master equation (8) for the density matrix can be rewritten in the form $\dot{\vec{\rho}}(t) = \mathcal{M}\vec{\rho}(t)$ where the density matrix ρ (here 17×17) is arranged as a vector $\vec{\rho}$ (with 289 components) and all the dynamics, coherent and dissipative, are included in the components of the large (289×289) matrix $\mathcal{M}$ (for details see Appendix). The spectral decomposition of this matrix,

$$\mathcal{M} \vec{\rho}_n = m_n \vec{\rho}_n, \quad (13)$$

gives access to various relaxation rates. It also yields the steady-state populations $\vec{\rho}(t \to \infty) = \vec{\rho}_{st} = \vec{\rho}_0$, which is the eigenvector corresponding to the zero eigenvalue $m_0 = 0$ [20].

If the effect of the baths is not weak a reduction to a classical rate equation is not allowed. Instead we should study the eigenvalue problem of Eq. (13). Its eigenvectors are superpositions of different eigenstates of H_{CF}. This is in particular true for the 0-family. We recall that due to degeneracies the eigenstates of H_{CF} corre-

sponding, e.g., to $m = \pm 6$ are the symmetric and antisymmetric coherent superpositions of (predominantly) the two J_z basis states, resulting in a vanishing expectation value $\langle J_z \rangle$ displayed in Fig. 2 a). Due to the dissipation this coherence may get destroyed. This scenario has been termed "environment-induced superselection" principle by Zurek [7, 8]. Decoherence selects favored "pointer" states which are stable under the influence of the environment [21]. These states are the steady-state eigenstates of the full quantum master equation which we will denote as $|\phi_m\rangle$ with $m = -J, -J+1, \ldots, J$. If the dissipation is strong these eigenstates are actually much closer to the original J_z basis states with non-vanishing expectation values $\langle J_z \rangle \approx \pm 6$. Similarly the states corresponding to $m = \pm 3$ get modified. The situation with strong dissipation is depicted in Fig. 2 b).

It is instructive to study the transition between the two limiting cases. We focus on the two stationary states of the doublet $|\phi_{+6}\rangle$ and $|\phi_{-6}\rangle$ and calculate their J_z expectation value. The result is depicted in Fig. 3. For weak dissipation, e.g., for small U the states reduce approximately to the H_{CF} eigenstates $|\psi_{6s}^0\rangle$ and $|\psi_{6a}^0\rangle$ with $\langle J_z \rangle \approx 0$, while for strong dissipation they approach the states with maximum expectation values $\langle J_z \rangle \approx \pm 6$. For low voltages the electrons do not have enough energy to scatter into higher excited states and the superposition states remains stable. For higher voltages exceeding $\sim 6\,\mathrm{mV}$ and nonzero temperature excitations are possible and the superposition is destroyed. In Fig. 3 we further note a special feature, namely a dip at $U = 7.7\,\mathrm{mV}$, since at this voltage the electrons are in resonance with the first excitation energy.

In the inset of Fig. 3 the dependence of the environment-induced superselection on the polarization of the tip is shown. Without polarization, the states have no preferred basis in which they evolve upon scattering of the electrons. But already a very small polarization in z-direction (mind the scale of the axes) is enough to drive the system to the pointer states with maximum $\langle J_z \rangle$.

The environment-induced superselection strongly influences the relaxation processes, which will be studied in the following section.

IV. RELAXATION TIME T_1

If the system is mainly in one of the two degenerate ground states, the relaxation time T_1 towards the steady state is given by the smallest non-zero eigenvalue of the matrix $\mathcal{M}$ (see Eq. (13)), corresponding to the eigenvector $\vec{\rho}_1 = (1, 0, \ldots, 0, -1)^T$. (Here we assumed an ordering such that the first and last entries of the eigenvector are the ground states). The inverse of the T_1 time, $1/T_1 = -m_1 = \Gamma_{-8 \to +8} + \Gamma_{+8 \to -8}$, accounts for all relaxation channels from one ground state to the other. Note that the switching rate $\Gamma_{-8 \to +8}$ from $|\phi_{-8}\rangle$ to $|\phi_8\rangle$ accounts for the direct transition but also all those via excited states. It thus differs from the rate Γ_{-88} of

the rate equations (12), which describes only the direct transition. The relation between the two switching rates $\Gamma_{-8 \to +8}$ and $\Gamma_{+8 \to -8}$ (and related lifetimes) follows from the steady state populations P_{-8} and P_{+8} of the two ground states, $\tau_{-8}/\tau_{+8} = \Gamma_{+8 \to -8}/\Gamma_{-8 \to +8} = P_{-8}/P_{+8}$.

A. Voltage dependence

To compare with the experiments of Ref. [1] we need to determine the coupling strength for tunneling of the reservoir electrons via the Ho atom. For this purpose we calculate the current I_{Th} from the dissipative part of the master equation (for details see Appendix). By comparing with the experiment we should be able to determine the coupling strength c_{TB}. However, the current I_{Th} describes only the current where electrons scatter due to the spin – angular momentum interaction. The total current, which in the experiments was always kept at $I_{Exp} = 1\,\mathrm{nA}$, includes a 'leakage' current $I_{Exp} = I_{Th} + I_{Leak}$. It can arise due to electrons tunneling directly between tip and bulk or due to electrons scattering with shells other than the $4f$ shell which forms the basis of the considered angular momentum states. By comparing the current which involves spin flips, and accordingly depends on the the spin state of the Ho atom, with the state-independent current we get a rough estimate. For the following discussion we assume that I_{Th} amounts for roughly 10% of the total current I_{Exp}, i.e. $I_{Th} = 0.1\,\mathrm{nA}$. For $U = 3\,\mathrm{mV}$ this is obtained for a coupling strength of $c_{TB} = 3.41 \cdot 10^6 (\mathrm{meV\,s})^{-1}$.

We are now ready to analyze the dependence of the relaxation time on the applied voltage. In Fig. 4 a) we plot the results for the temperature $T = 0.7\,\mathrm{K}$ chosen in the experiments, and for comparison also at several higher temperatures $T = 1.4\,\mathrm{K}$, $T = 3.5\,\mathrm{K}$, and $T = 7\,\mathrm{K}$. We compare the T_1 time, as obtained from the numerical solution of the full quantum master equation, and the result obtained from the approximate rate equations (12) in the basis of H_{CF} eigenstates. Similarly we compare in Figs. 4 b) the J_z expectation values of the steady state solutions of the master equation and those of the H_{CF} eigenstates for two different values of U. For reasons of numerical stability we include in all our simulations the effect of a very weak magnetic field applied in z-direction ($B_z = 10^{-8}\,\mathrm{T}$). Otherwise the two ground states get completely decoupled within our numerical precision, and divergences appear, or the reduced density matrix is no longer positive semidefinite.

Focusing on low temperature, $T = 0.7K$, we note that for low voltages, $U \lesssim 3\,\mathrm{mV}$, the six lowest lying steady states of the full quantum master equation have very similar properties as the H_{CF} eigenstates. In this regime transitions between the two ground states $|\psi_8^+\rangle$ to $|\psi_{-8}^-\rangle$ are caused mostly by the (weak) symmetry-breaking magnetic field and are thus voltage independent. The full master equation yields shorter lifetimes
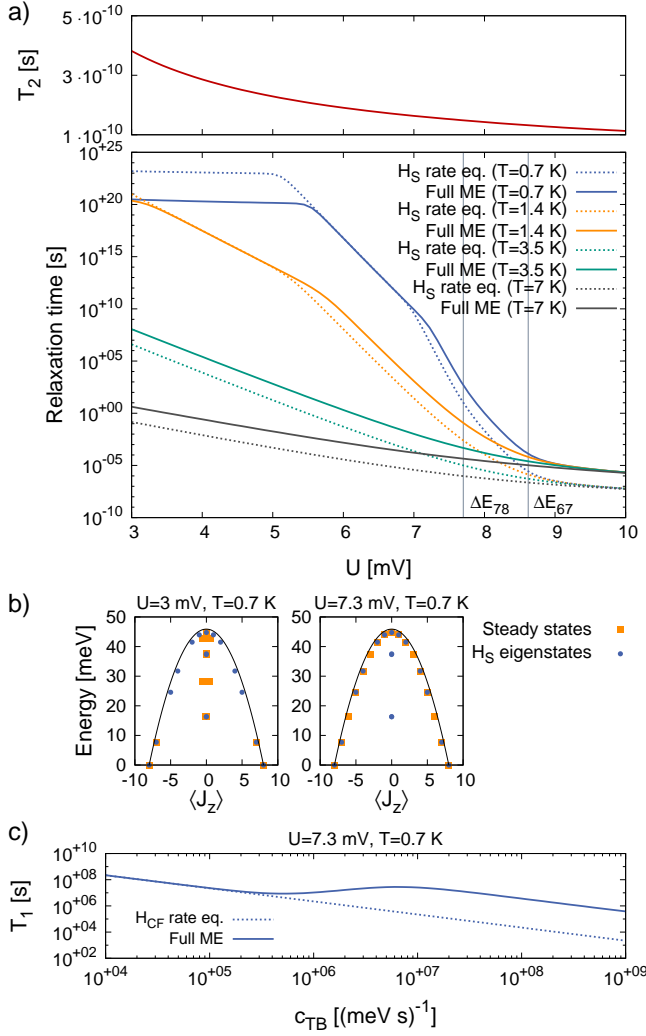
FIG. 4. a) Relaxation time T_1 and decoherence time T_2 of the two ground states versus the applied voltage U obtained from the full quantum master equation (13)(full lines) and the rate equation (12) based on H_{CF} eigenstates (dotted lines). A weak magnetic field $B_z = 10^{-8}$ T is applied, the temperatures are $T = 0.7$ K, $T = 1.4$ K, $T = 3.5$ K and $T = 7$ K, and the coupling strength is $c_{TB} = 3.41 \cdot 10^6 (\text{meV s})^{-1}$. b) Energy expectation values versus the expectation values $\langle J_z \rangle$ for the steady states of the full quantum master equation and for the H_{CF} eigenstates at $T = 0.7$ K for $U = 3$ mV and $U = 7.3$ mV. c) Relaxation time T_1 versus the coupling strength c_{TB} as obtained from the full quantum master equation and the rate equation for $T = 0.7$ K and $U = 7.3$ mV.

than the rate equation in this regime, because of additional coherent transitions contained in the full theory.

At higher voltages we observe for $T = 0.7$ K and $T = 1.4$ K in (the semi-log plot of) Fig.4 a) an exponentially activated behavior. In this regime the full master equation and the rate equation yield very similar results. Here the main switching channel is via the first excited states, $|\phi_7\rangle$ or $|\phi_{-7}\rangle$, followed by a fast decay to the other ground state on the other side of the parabola. Since

the first step is the bottleneck of the process we have $1/T_1 \approx \Gamma_{87} + \Gamma_{-8-7}$. For an estimate we ignore the effect of the tip polarization and of a magnetic field (i.e. $\Gamma_{87} \approx \Gamma_{-8-7}$) and get

$$\Gamma_{87} = c_{TB} |\langle \psi_7^- | J_- | \psi_8^+ \rangle|^2 \cdot \zeta(E_7 - E_8 - eU) \quad (14)$$

$$\approx 16 c_{TB} \cdot \frac{(E_7 - E_8 - eU)}{e^{(E_7 - E_8 - eU)/k_B T} - 1} \quad (15)$$

For still higher voltages, $U > 7$ mV, the results obtained in the two approaches differ again. In this regime, in the frame of the rate equation excitations to the symmetric and anti-symmetric H_{CF}-eigenstates $|\psi_{6s}^0\rangle$ and $|\psi_{6a}^0\rangle$ become possible. These two states have high transition rates between each other and thus provide a 'shortcut' for the decay. However, in the full master equation these superpositions states are replaced by the steady states $|\phi_{+6}\rangle$ and $|\phi_{-6}\rangle$, with properties illustrated in Figs. 3 and 4 b), which in this parameter regime are actually close to $\langle J_z \rangle = \pm 6$ states. They are weakly coupled, and the shortcut is no longer open, which increases the relaxation time.

For even higher voltages, $U > 8.6$ mV, tunneling electrons have enough energy to overcome also the second energy excitation gap of $\Delta E_{67} = E_6 - E_7 \approx 8.6$ meV, which is the largest gap of the system. From this point on, sequential scattering over the top of the parabola is the main transition channel, and the slope of $T_1(U)$ versus U changes.

At higher temperatures, the different regimes get smeared out, as can be seen in the plot of Fig. 4, especially for $T = 3.5$ K and $T = 7$ K. In this regime the main transition channel is always via higher excited states. For voltages larger than $U \approx 9$ mV the results for all temperatures are very similar, because in all cases most of the electron scattering leads to the transition over the top of the parabola. Again, the rate equations overestimate the role of transitions via the 'shortcut' states $|\psi_{6s}^0\rangle$, $|\psi_{6a}^0\rangle$, $|\psi_{3s}^0\rangle$ and $|\psi_{3a}^0\rangle$.

In Fig. 4 c) we investigate the dependence of the lifetime on the coupling strength c_{TB} for low temperature and $U = 7.3$ mV. From the rate equations we find simply that T_1 time decreases proportional to $1/c_{TB}$. But the solution of the full quantum master equation yields different results. In the considered regime excitations to the $|\phi_{+6}\rangle$ and $|\phi_{-6}\rangle$ play a role. The coherence leading to these superposition states is increasingly destroyed with growing coupling strength. As a result in the range $10^5 (\text{meV s})^{-1} \leq c_{TB} \leq 10^7 (\text{meV s})^{-1}$ the stronger coupling even stabilizes the system by decoupling the two sides of the parabola.

B. Further details of the experiments

To compare with the experiments of Ref. [1], two further effects have to be taken into account. First,
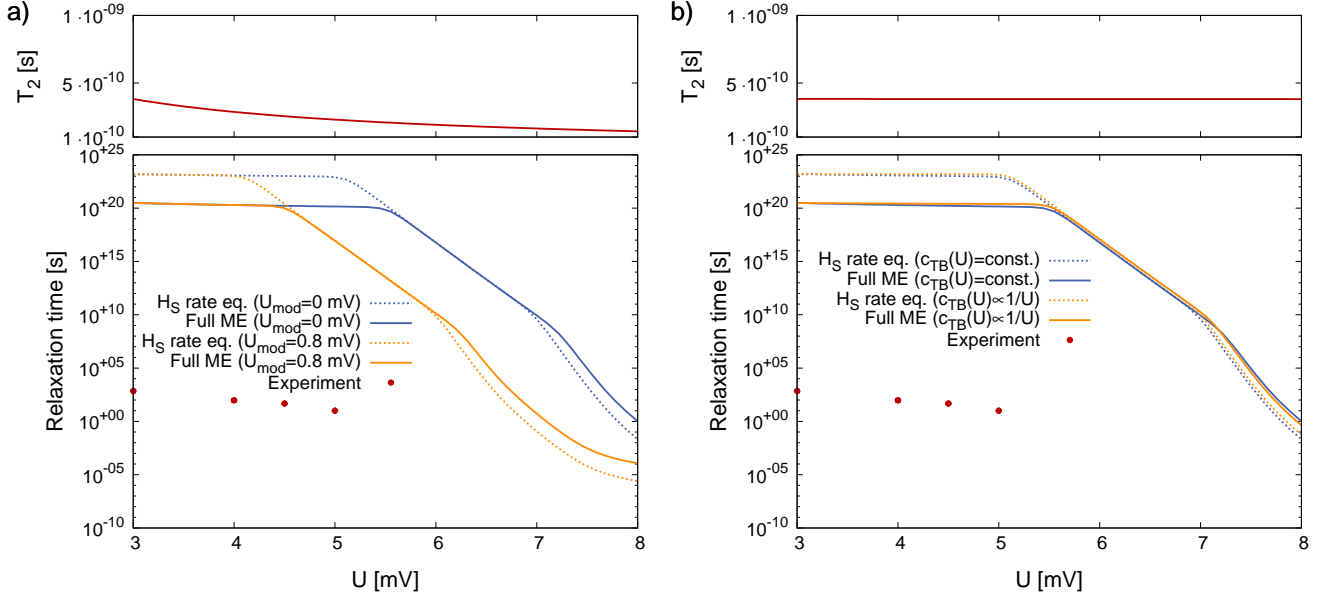
FIG. 5. Relaxation time T_1 and decoherence time T_2 of the two ground states versus the applied voltage U in a weak magnetic field $B_z = 10^{-8}$ T at $T = 0.7$ K for the full master equation solution and the rate equation (12) with the H_{CF} eigenstates. a) With and without modulation voltage $U_{mod} = 0.8$ mV. b) With and without tip distance correction. For comparison the experimental data are shown in red. The error bars are too small to be visible.

in the experiment the applied voltage was modulated, $U_{tot}(t) = U + \sqrt{2}U_{mod}\cos(\omega t)$, with $U_{mod} = 0.8$ mV. The frequency of the modulation, $\omega = 720$ Hz, is several orders of magnitude faster than the timescales of interest. We model this fast oscillation by suitably averaging the correlation functions with the distribution $h(U') = 1/\pi \left[2(eU_{mod})^2 - (eU')^2\right]^{-1/2}$ for $|U'| \leq \sqrt{2}U_{mod}$ and $h(U') = 0$ otherwise [23]. This means, e.g.

$$\tilde{C}_{+-}^{TB}(\Lambda_{nm}) = c_{TB}\frac{1}{2}(1+\eta)$$
$$\times \int dU' \zeta(\Lambda_{nm} + eU^T + eU')h(U'). \quad (16)$$

The effect on the lifetimes is shown in Fig. 5 a). In essence, the modulation amounts to a shift $U \to U + \sqrt{2} \cdot U_{mod}$, by approximately 1.1mV.

Second, in the experiment the voltage-induced tunnel current was measured, and in fact, by adjusting the distances between tip and electrode, was kept fixed at the value $I_{Exp} = 1$ nA. To keep the current fixed for different voltages U, we allow in the simulations $c_{TB}(U)$ to be voltage dependent. We checked numerically that the tunnel contact behaves close to Ohmic, $I_{Th} \approx U/R_{Tun}$. We therefore adjust the coupling $c_{TB}(U) \propto 1/U$ to keep the current constant. We recall that an estimated 90% of the current is leakage current. With $c_{TB}(U = 3$ mV$) = 3.41 \cdot 10^6$(meV s)$^{-1}$ we arrive at $I_{Th} = 0.1$ nA. We will proceed using these values in all simulations reported below. All this being said and done, we note that the effect of the adjustment, which is included in Fig. 5 b), is weak.

V. DEVIATIONS FROM THE IDEAL SITUATION

When comparing the calculated T_1 times with the experimental data, as illustrated in Figs. 5, we note that the theory produces far too long times. Therefore, we need to take a closer look at the experiment and possible deviations from the ideal situation assumed so far.

A. Scattering of bulk electrons

Up to now we ignored the effect of bulk electrons scattering from the Ho atom, and the question arises whether it could be the source of the mismatch between theory and experiment. The scattering processes are easily included in the quantum master equation, and their effects are illustrated in Fig. 6. In the first panel we show how the relaxation time depends on the coupling strength c_{BB} for a fixed value of the tunneling strength $c_{TB} = 3.41 \cdot 10^6$(meV s)$^{-1}$ and voltage $U = 5$ mV. As long as c_{BB} is smaller than c_{TB} the lifetime remains nearly unchanged. For stronger c_{BB}, the scattering of bulk electrons leads to suppression of coherent transitions and thus to *longer* lifetimes. This arises because of the low temperature of the bulk electrodes, which cools the system into the ground states, whereas the tunneling electrons due to the applied voltage have enough energy to excite the system. The combination of voltage-dependent tunneling and voltage independent scattering is illustrated in Fig. 6 b) (including the effects of modulation voltage broadening and tip distance
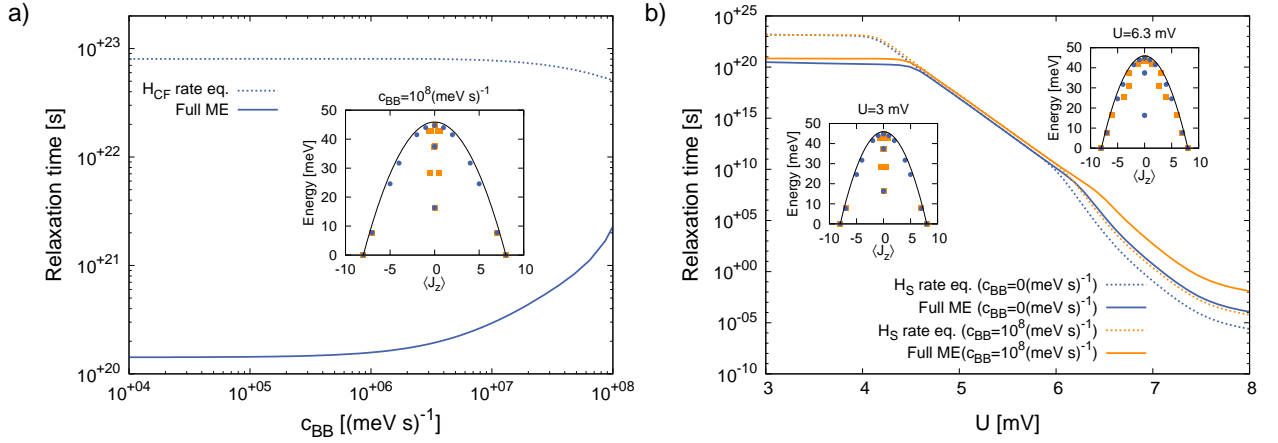
FIG. 6. a) Relaxation time T_1 versus the bulk electron scattering strength c_{BB} as obtained from the full master equation (13) and the rate equation (12) based on H_{CF} eigenstates. The parameters are $U = 5$ mV, $B_z = 10^{-8}$ T, $c_{TB} = 3.41 \cdot 10^6$ (meV s)$^{-1}$. b) Relaxation time T_1 versus the voltage U for the model with modulation voltage broadening and tip distance correction with and without bulk electron scattering strength $c_{BB} = 1.0 \cdot 10^7$ (meV s)$^{-1}$.
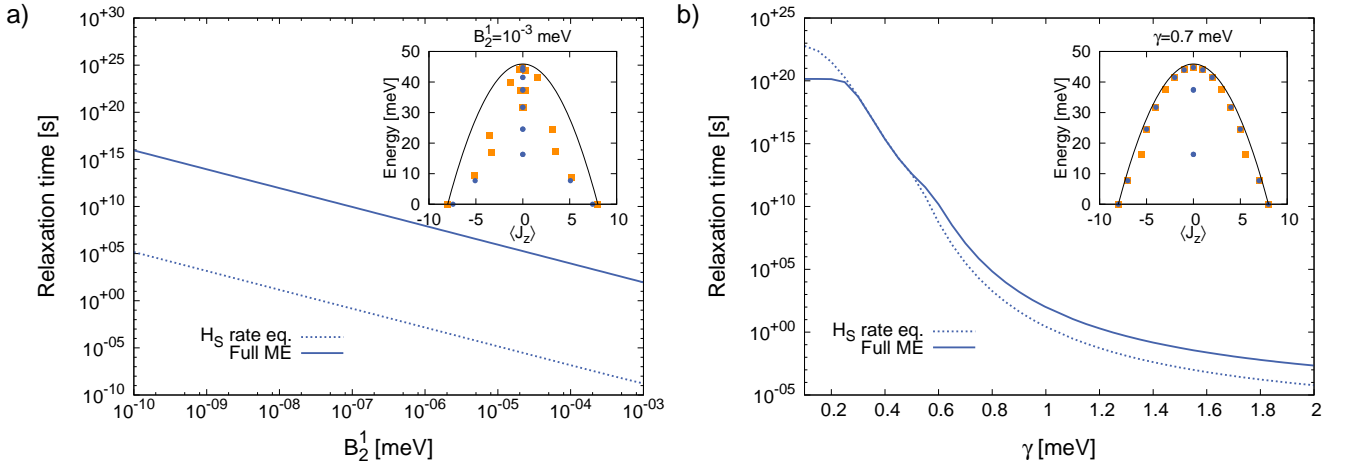

FIG. 7. Relaxation time T_1 of the two ground states under the influence of deviations from the perfect situation. We compare the results obtained from the full master equation (13) and the rate equation (12) based on the H_{CF} eigenstates. a) T_1 versus Stevens parameter B_2^1 characterizing the deviation from the perfect trigonal symmetry. b) T_1 versus the strength of Gaussian broadening γ chosen to account for further lifetime broadening effects. In both plots we choose the parameters $U = 5$ mV and $B_z = 10^{-8}$ T. The insets show the J_z expectation value of the steady states and the H_{CF} eigenstates.

correction described above). We assume a bulk electron scattering strength $c_{BB} = 1.0 \cdot 10^7$ (meV s)$^{-1}$ which is slightly higher than the tunneling coupling strength $c_{TB} = 3.41 \cdot 10^6$ (meV s)$^{-1}$. Again we note the increase of the lifetime as a consequence of the scattering.

B. Breaking the C_{3v}-symmetry

As an example of a symmetry breaking term, we consider the effect of the C_{3v}-symmetry-breaking term of the Stevens operators, $B_2^1 \cdot O_2^1 = B_2^1 \cdot [J_z, J_+ + J_-]_+$ [22]. This term arises if the tip is not perfectly centered over the Ho atom, or if nearby surfaces or imperfections in the crystal break the symmetry. It breaks all the rota-

tional symmetries of the system. A magnetic field in the xy-plane would have a similar effect.

The symmetry-breaking parameter B_2^1 is varied in Fig. 7 a) between 10^{-10} meV and 10^{-3} meV, which is still orders of magnitude lower than the leading crystal-field term $B_2^0 = -0.239$ meV. As a result of the symmetry breaking the eigenstates of H_{CF} get mixed, and the protection against direct transitions is lost. In Fig. 7 a), the voltage is chosen to be $U = 5$ meV, so the leading transition is directly between the two ground states. With rising strength of B_2^1 the relaxation time decreases $T_1 \propto (B_2^1)^{-2}$. In the frame of the rate equations the switching arises since electron tunneling directly couples the two states. In the frame of the full master equation scattering of electrons destroys the phase coherence of

these superpositions and the resulting expectation values $\langle J_z \rangle$ of the steady states are closer to the parabola, characteristic for the H_{CF} eigenbasis (see the ground states of the inset of Fig. 7 a)). This means, that the symmetry protection gets restored and the lifetimes increase drastically. All this depends on the coupling strength c_{TB}, which is the important parameter for the superselection (see Fig. 4 c)). Unfortunately, the parameter B_2^1 is not independently accessible in the experiment, and it is difficult to draw more precise conclusions.

C. Noise in the circuit

To account for the influence of further perturbations, such as thermal noise in the electronics, we introduce a lifetime broadening. Specifically we average the results obtained so far, assuming a Gaussian broadening of the tunneling electron energy distribution $g(\delta E, \gamma) = 1/\sqrt{2\pi\gamma^2} \exp[-\delta E^2/(2\gamma^2)]$ with a width characterized by the parameter γ [23]. Its influence on the lifetime T_1 is visualized in Fig. 7 b). The relaxation time is strongly reduced by this broadening because the broadening allows excitations into one of the $|\phi_7\rangle$ or $|\phi_{-7}\rangle$ states, followed by a subsequent decay to the other ground state.

By fitting the parameters characterizing the two deviations from the ideal situation we manage to obtain results for the T_1 times close to the the experimental ones (see Fig. 8). We plot results for two values of the temperature $T = 0.7\,\mathrm{K}$ and $T = 1.4\,\mathrm{K}$, where the first one is the bath temperature in the experiment, while the second is chosen to account for some electron heating induced by the current. (An increased temperature alone would not be sufficient to explain the discrepancy between the simulations and the experiment.) Although with the fitting we reached a reasonable agreement with experiment we have to acknowledge that the fit is not conclusive, since the number of data points is too low to determine the parameters independently.

D. Magnetic field dependence

Next, we investigate the effect of an applied or stray magnetic field B_z which is probably present in the experiments. Its influence depends strongly on the values of the other parameters. In Fig. 9 a) we show the resulting modification for the regime where the main transition, although with small rate, is directly between the states $|\psi_8^+\rangle$ and $|\psi_{-8}^-\rangle$. We choose $U = 5\,\mathrm{mV}$, i.e., we are still in the regime of voltage-independent relaxation time of Fig. 4 a). As shown in Fig. 9 a) the lifetime is strongly reduced by the symmetry breaking magnetic field B_z, since the symmetry protection of the two ground states is lost. This behavior is obtained both from the rate equation and the solution of the quantum master equation.

Interestingly, as illustrated by Fig. 9 b), the behavior can be completely different for different parameters. In
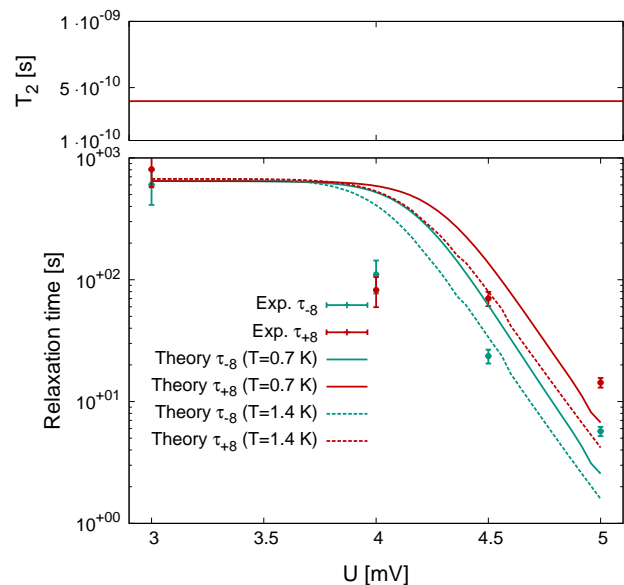
FIG. 8. Relaxation time T_1 and decoherence time T_2 of the two ground states versus the applied voltage U at $T = 0.7\,\mathrm{K}$ and $T = 1.4\,\mathrm{K}$ for the modulation amplitude $U_{mod} = 0.8\,\mathrm{mV}$, lifetime broadening $\gamma = 0.95\,\mathrm{meV}$, magnetic field $B_z = 1 \cdot 10^{-8}\,\mathrm{T}$, symmetry breaking $B_2^1 = 4 \cdot 10^{-4}\,\mathrm{meV}$, and tip spin polarization $\eta = 0.15$. We compare the results obtained from the full master equation (13) (solid lines) and the rate equation (12) based on the H_{CF} eigenstates (dashed lines). The theoretical values are compared with the state-dependent data from the experiment with error bars indicating the statistical errors of the measurement.

this example the lifetime increases when a field is applied. For the chosen parameters the B_z field stabilizes the J_z eigenstates and reduces the switching, which otherwise would be induced by the symmetry breaking term B_2^1. We conclude that a detailed study of the magnetic field dependence should provide a better understanding of the different perturbations acting on the Ho adatom.

E. Alternative choice of the crystal-field parameters

In a recent publication Donati *et al.* [6] reported about x-ray absorption spectroscopy (XAS) and magnetic circular dichroism (XMCD) measurements performed with Ho on Pt(111). The results could be fitted with a crystal-field Hamiltonian of the form (1) but with only the coefficients $B_2^0 = -140\,\mu\mathrm{eV}$ and $B_4^0 = 1\,\mu\mathrm{eV}$ differing from zero, which differs significantly from what Miyamachi *et al.* [1] used, and what we assumed so far in this paper. To simulate the lifetimes in our theory with these parameters, we add a small $B_4^3 \approx 0.3\,\mu\mathrm{eV}$ which we take from Miyamachi *et al.* [1], because otherwise the ground states decouple completely. With these inputs, we arrive at the level scheme shown in the inset of Fig. 10. Most important we note that the ground states are now
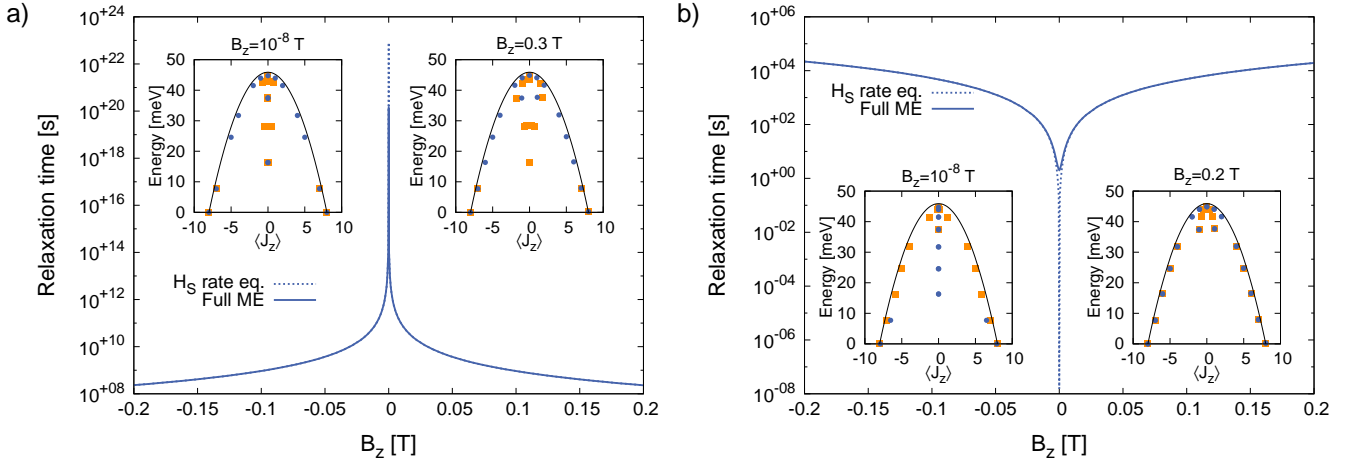
FIG. 9. Relaxation time T_1 of the two ground states versus a magnetic field B_z as obtained from the full master equation (13) and the rate equations (12) based on H_{CF} eigenstates. The insets show the expectation value of J_z for the two descriptions. a) Results for the ideal model for $U = 5\,\mathrm{mV}$. b) Results with symmetry-breaking and Gaussian broadening corresponding to the fits of Fig. 8, i.e., $U_{mod} = 0.8\,\mathrm{mV}$, $\gamma = 0.95\,\mathrm{meV}$, and $B_2^1 = 4 \cdot 10^{-4}\,\mathrm{meV}$.
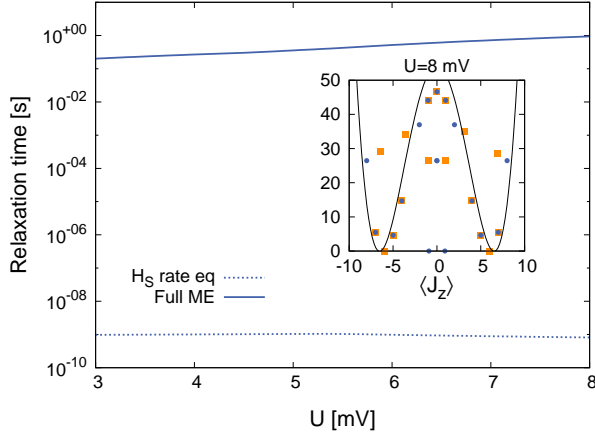

FIG. 10. Relaxation time T_1 of the two ground states versus the voltage U as obtained from the full master equation and from the rate equations (12) based on H_{CF} eigenstates for $B_z = 10^{-8}\,\mathrm{T}$. The inset shows the expectation value of J_z for the two descriptions for $U = 8\,\mathrm{mV}$. The black line shows the function $f(J_z) = -140\,\mu\mathrm{eV} \cdot O_2^0 + 1\,\mu\mathrm{eV} \cdot O_4^0 + \mathrm{const.}$.

the $|\psi_{6s}^0\rangle$ and $|\psi_{6a}^0\rangle$, which are much stronger coupled (not symmetry-protected) than the states $|\psi_8^+\rangle$ and $|\psi_{-8}^-\rangle$ and hence should have much shorter lifetimes. We analyzed the relaxation rate in the same way as for the other model, with results shown in Fig. 10. We note that the solution of the rate equation yields very short relaxation times of the order of nanoseconds. On the other hand, the simulation based on the full master equation yields longer lifetimes. The reason is again the environment-induced superselection which destroys the superpositions. The differences between the two sets of eigenstates are pronounced, as can be seen in the inset of Fig. 10. In fact the difference between the two theoretical approaches is even

more pronounced than found in the model based on the parameters of Miyamachi et al.. We further note from Fig. 10 that higher voltages even stabilize the ground states, because the excited states couple less to the states on the opposite side of the parabola than $|\psi_{+6}^0\rangle$ and $|\psi_{-6}^0\rangle$ do, and hence the excitation of those states reduces the transition rate. This voltage dependence is in stark contrast to the observations made by Miyamachi et al. [1], where the lifetimes decrease with increasing voltages.

The comparison of theory and experiment on the voltage dependence of the relaxation time supports the Stevens parameters used by Miyamachi et al. [1]. They were derived by ab initio DFT calculations for a situation where individual Ho atoms were adsorbed on high-symmetry fcc sites on the surface of Pt(111). In contrast, the experiments of Donati et al. [6] were performed with a high coverage of Ho atoms of 0.04 monolayers occupying a mixture of hcp and fcc sites. Further investigations are needed to clarify whether this is the origin of the differing results.

VI. DECOHERENCE TIME T_2

The decoherence time T_2 is the time scale on which the phase information in a coherent superposition, here specifically of the states $|\psi_8^+\rangle$ and $|\psi_{-8}^-\rangle$, gets lost. In the quantum master equation treatment of the problem, T_2 is obtained from the decay rate of the off-diagonal matrix element ρ_{+8-8}, which is given by the corresponding matrix element in the matrix $\mathcal{M}$,

$$
\begin{aligned}
1/T_2 &= -\mathcal{M}_{8-8\to 8-8} \\
&\approx 4c_{TB}\, \langle\psi_8^+|J_z|\psi_8^+\rangle\, \langle\psi_{-8}^-|J_z|\psi_{-8}^-\rangle\, \zeta(-eU) \\
&\approx 264\, c_{TB}\, eU.
\end{aligned}
\tag{17}
$$

The resulting T_2 times are plotted for different parameters in Figs. 4, 5 and 8. It turns out that the T_2 time depends mostly on the current, i.e., on the number of scattered electrons. Roughly one can argue that each scattered electron dephases the superposition state, independent of the energy of the electron. Thus, we detect only in Fig. 4 a) and Fig. 5 a) a dependence of T_2 on the voltage U, because in all other plots the current is kept constant (achieved by the adjustment of $c_{TB}(U)$). We note that the decoherence times T_2 are always very short ($\sim 10^{-10}$ s) making the considered memory unsuitable as a quantum mechanical bit (qubit). Additionally, we found that T_2 does not depend on the symmetry breaking B_2^1, the broadening γ, or the magnetic field B_z. If the voltage is set to zero, all terms $\tilde{C}_{\nu\nu'}^{\alpha\alpha'}(\pm\Lambda_{nm})$ are similarly important. Hence T_2 is given by

$$1/T_2 = - M_{8-8\to8-8}$$
$$\approx 4(\sum_{\alpha\alpha'} c_{\alpha\alpha'}) \langle\psi_8^+|J_z|\psi_8^+\rangle \langle\psi_{-8}^-|J_z|\psi_{-8}^-\rangle \zeta(0)$$
$$\approx 264\, k_B T \sum_{\alpha\alpha'} c_{\alpha\alpha'}. \tag{18}$$

If one assumes that $\sum_{\alpha\alpha'} c_{\alpha\alpha'} \approx 10^6 (\text{meV s})^{-1}$ and the temperature is $T = 1\,\text{K}$, the decoherence time is roughly 10^{-8} s.

VII. INITIALIZATION

We have seen that the relaxation time depends strongly on various parameters. In this section we will demonstrate that by switching parameters suitably we can initialize a specific angular momentum state [24]. This enables the writing process if the Ho atom is used as a memory. As a specific example we study what happens to the state $|\psi_{-8}^-\rangle$ when we pulse the system for a time t_p with a voltage U and then let the system relax for $1\,\mu$s without a voltage applied. After the relaxation, the population of the state $|\psi_8^+\rangle$ is measured, which provides the information about the switching probability $S_{-8\to8}(U, t_p)$.

In Fig. 11, the switching probability $S_{-8\to8}(U, t_p)$ as obtained from the quantum master equation is plotted versus the strength of the applied voltage pulse for different spin polarizations η of the tip. (We neglect again the influence of the bulk electron scattering.) For $U > 20\,\text{mV}$ the value of $S_{-8\to8}(U, t_p)$ may get close to 1, i.e., the pulse flips the Ho atom with a high probability into the state $|\psi_8^+\rangle$. On the other hand, a pulse with opposite voltage $U < -20\,\text{mV}$ leaves the state with high probability in the state $|\psi_{-8}^-\rangle$. Thus, both ground states can be prepared by applying voltage pulses with either sign. For voltages between $-10\,\text{mV} \lesssim U \lesssim 10\,\text{mV}$ basically no switching of the Ho spin state is induced, $S_{-8\to8}(U, t_\text{p}) \approx 0$. Around $U = 20\,\text{mV}$ the switching is strongest as long as $\eta \neq 0$. For an unpolarized tip, $\eta = 0$, a pulse with high voltage produces a balanced population of the two ground states.

The upper inset of Fig. 11 shows the dependence of the switching probability $S_{-8\to8}(U, t_p)$ on the spin polarization η for optimum conditions $U = 20\,\text{mV}$ and pulse time $t_p = 2.5\cdot10^{-7}$ s. As one could expect, the higher the polarization, the better the initialization. But, the switching between the ground states also requires a certain number of electrons, which increases with longer pulse time t_p, as displayed in the lower inset of Fig. 11. For the optimal voltage of $U = 20\,\text{mV}$ we calculate a current of $I_{Th} \approx 0.75\,\text{nA}$. A pulse time of $t_p \approx 250\,\text{ns}$ implies then that around 1100 electrons are needed to prepare the atom in one state. By changing the tip distance in the experiment, this dependence could be probed.

Our simulations suggest that it is possible to prepare the system in a required state using pulse times of a few hundreds nanoseconds with high fidelity as long as the tip polarization is large enough. The required pulse time depends strongly on the parameter c_{TB}. Thus, an experiment with different pulse lengths could help to determine this value.
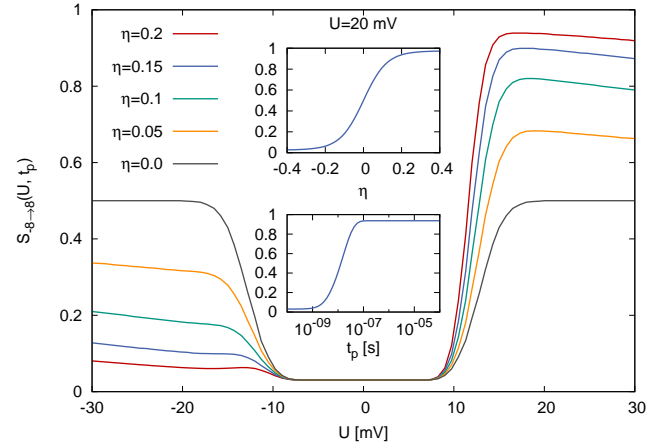

FIG. 11. The probability for switching from $|\psi_{-8}^-\rangle$ to $|\psi_8^+\rangle$ versus the applied pulse voltage for different values of the tip polarization η and a pulse time of $t_p = 2.5 \cdot 10^{-7}$ s. The upper inset shows the switching probability versus the tip polarization for pulse strength $U = 20\,\text{mV}$ and pulse time $t_p = 2.5 \cdot 10^{-7}$ s. The lower inset shows the dependence on the pulse time t_p for pulse strength of $U = 20\,\text{mV}$ and $\eta = 0.2$.

VIII. CONCLUSION

When investigating the dynamics of the angular momentum states of Ho on Pt(111) we found that in an important regime of parameters the system behaves deeply quantum mechanically and cannot be described by a rate equation for transitions between the eigenstates of the crystal-field Hamiltonian H_{CF}. Rather the system has to be treated by the full quantum master equation. Its steady-state basis in general differs from the H_{CF} eigenstates, which is an example of the "environment-induced

superselection" principle [7, 8]. We analyzed how the relaxation time T_1 depends on various parameters of the system. In ideal situations at low temperatures it should be extremely long. In contrast the decoherence time T_2 is always very short. We further described a method to initialize the system in one of the two ground states by suitable voltage pulses.

By a proper choice of the parameters describing deviations from the ideal situation we could roughly fit the experiments, with still remarkably long lifetimes. Our analysis shows that if the parameters could be improved and controlled more precisely the system would acquire even longer lifetimes than observed already. The system therefore promises to be useful as a single-atom memory with the possibility to write into the memory by very short pulses of electric currents with high fidelity.

At this stage, we have to conclude that there are too few experimental data available to determine the parameters independently. A further detailed investigation of the coupling parameter c_{TB} and the other parameters is required to identify the main perturbation which limits the lifetime of the Ho adatom in the experiment. The lifetime depends strongly on an applied magnetic field. The analysis of this effect would help obtaining the missing information on the parameters.

IX. ACKNOWLEDGMENTS

Appendix A: Stevens operators and parameters

For convenience we list here the Stevens operators which are needed to describe the system Ho on Pt(111) [1, 12]

$$O_2^0 = 3J_z^2 - J(J+1), \tag{A1}$$

$$O_4^0 = 35J_z^4 - 30J(J+1)J_z^2 + 25J_z^2 - 6J(J+1) \\ + 3J^2(J+1)^2, \tag{A2}$$

$$O_4^3 = \frac{1}{4}\left[J_z(J_+^3 + J_-^3) + (J_+^3 + J_-^3)J_z\right], \tag{A3}$$

$$O_6^0 = 231J_z^6 - 315J(J+1)J_z^4 \\ + 735J_z^4 + 105J^2(J+1)^2 J_z^2 - 525J(J+1)J_z^2 \\ + 294J_z^2 - 5J^3(J+1)^3 + \\ 40J^2(J+1)^2 - 60J(J+1), \tag{A4}$$

$$O_6^3 = \frac{1}{4}\left[(11J_z^3 - 3J(J+1)J_z - 59J_z)(J_+^3 + J_-^3) \\ + (J_+^3 + J_-^3)(11J_z^3 - 3J(J+1)J_z - 59J_z)\right], \tag{A5}$$

$$O_6^6 = \frac{1}{2}\left[J_+^6 + J_-^6\right]. \tag{A6}$$

We also list the parameters which were obtained from ab-initio simulations and listed in Ref. 1.

Anisotropy constant	value
B_2^0	-239 μeV
B_4^0	86 neV
B_4^3	293 neV
B_6^0	0.186 neV
B_6^3	-1.967 neV
B_6^6	0.630 neV

TABLE I. Anisotropy parameters as used in Ref. 1.

Appendix B: Setting up the matrix $\mathcal{M}$

In this section we present the approach we use to solve the quantum master equation in Born-Markov approximation. By using the explicit time dependence of the system operators $J_\nu(t)$ in the interaction picture we evaluate the time integrals including the correlation functions of the master equation [25, 26]

$$S_{\nu\nu'}^{\alpha\alpha'}(\pm\tau) \equiv \int_0^\infty d\tau\, C_{\nu\nu'}^{\alpha\alpha'}(\pm\tau) e^{-iH_S\tau} J_j e^{iH_S\tau}. \tag{B1}$$

In the eigenbasis of $H_S |n\rangle = E_n |n\rangle$, the matrix elements of $S_{\nu\nu'}^{\alpha\alpha'}(\pm\tau)$ become

$$\langle n| S_{\nu\nu'}^{\alpha\alpha'} \pm tau) |m\rangle = \int_0^\infty d\tau\, C_{\nu\nu'}^{\alpha\alpha'}(\pm\tau) \\ \langle n| e^{-iH_S\tau} |n\rangle \langle n| J_{\nu'} |m\rangle \langle m| e^{iH_S\tau} |m\rangle \tag{B2}$$

$$= \langle n| J_{\nu'} |m\rangle \int_0^\infty d\tau\, C_{\nu\nu'}^{\alpha\alpha'}(\pm\tau) e^{i\Lambda_{nm}\tau} \tag{B3}$$

$$= \langle n| J_{\nu'} |m\rangle \left[\frac{1}{2}\tilde{C}_{\nu\nu'}^{\alpha\alpha'}(\pm\Lambda_{nm}) - iP\int \frac{d\omega}{2\pi} \frac{\tilde{C}_{\nu\nu'}^{\alpha\alpha'}(\omega)}{\Lambda_{nm} \mp \omega}\right]. \tag{B4}$$

Here, $\Lambda_{nm} = E_m - E_n$ are the energy differences and the tilde over the correlation functions indicate Fourier transforms. The imaginary parts of this equation vanish in the Born-Markov approximation because in the master equation complex conjugate terms are summed.

For a formulation that can be implemented efficiently in source code, the quantum master equation is rewritten in the form

$$\frac{d}{dt}\vec{\rho} = \mathcal{M}\vec{\rho}. \tag{B5}$$

Here $\vec{\rho} = \text{vec}\{\rho\}$ denotes the column-vectorization of the matrix ρ, meaning that the $(i+1)^{\text{th}}$ column of the matrix is written below the other i ones. The supermatrix M

has the dimension $\dim(\rho)^2$, which implies an extension of the complexity, but on the other hand the solution of this equation is possible with standard numerical tools. With the help of the relation [27]

$$\text{vec}\{AXB\} = (A \otimes B^T)\text{vec}\{X\}, \tag{B6}$$

where A, X and B are matrices, the transformation of quantum master equation into the wanted type is possible. The symbol $\otimes$ is the Kronecker-product of the matrices is defined as

$$A \otimes B = \begin{bmatrix} a_{11}B & \cdots & a_{1n}B \\ \vdots & \ddots & \vdots \\ a_{m1}B & \cdots & a_{mn}B \end{bmatrix}. \tag{B7}$$

For the problem considered in this paper we get

$$\mathcal{M} = \mathcal{M}_C + \mathcal{M}_D \tag{B8}$$

$$\mathcal{M}_C = i\left(\mathbb{1} \otimes H_S^T - H_S \otimes \mathbb{1}\right) \tag{B9}$$

$$\mathcal{M}_D = -\sum_{\substack{\nu,\nu'=+,-,z \\ \alpha,\alpha'=T,B}} \left[\left(J_\nu S_{\nu\nu'}^{\alpha\alpha'}(+\tau) \otimes \mathbb{1}\right)\right.$$
$$-\left(S_{\nu\nu'}^{\alpha\alpha'}{}^\sigma(+\tau) \otimes (J_\nu)^T\right)$$
$$\left.+\left(\mathbb{1} \otimes [S_{\nu\nu'}^{\alpha\alpha'}(-\tau)J_\nu]^T\right) - \left(J_\nu \otimes [S_{\nu\nu'}^{\alpha\alpha'}(-\tau)]^T\right)\right], \tag{B10}$$

where $\mathcal{M}_C$ contains the coherent part of the master equation and $\mathcal{M}_D$ the dissipative part.

Appendix C: Calculating the Current

The current is given by the time-derivative of the number of particles of the tip $N_T(t) = \sum_{k\sigma} c_{k\sigma}^{T\dagger}(t)c_{k\sigma}^T(t)$,

$$I_{Th}(t) = e\frac{d}{dt}\langle N_T(t)\rangle = ie\langle[H, N_T(t)]\rangle. \tag{C1}$$

In the commutator $[H, N_T(t)]$ only the coupling Hamiltonian H_C survives, which leads to

$$I_{Th} = -ie\sum_{kk'} t^{TB}\left(\langle J_+ c_{k\downarrow}^{B\dagger} c_{k'\uparrow}^T\rangle + \langle J_- c_{k\uparrow}^{B\dagger} c_{k'\downarrow}^T\rangle\right.$$

$$+ \langle J_z \left[c_{k\uparrow}^{B\dagger} c_{k'\uparrow}^T - c_{k\downarrow}^{B\dagger} c_{k'\downarrow}^T\right]\rangle$$
$$- \langle J_+ c_{k\downarrow}^{T\dagger} c_{k'\uparrow}^B\rangle - \langle J_- c_{k\uparrow}^{T\dagger} c_{k'\downarrow}^B\rangle$$
$$\left.- \langle J_z \left[c_{k\uparrow}^{T\dagger} c_{k'\uparrow}^B - c_{k\downarrow}^{T\dagger} c_{k'\downarrow}^B\right]\rangle\right). \tag{C2}$$

This form of the current bears similarity to terms in the master equation. It contains all the tunneling events from the tip to the bulk with a positive sign and those in opposite direction with a negative sign. Proceeding similar to the steps used for the dissipative part $\mathcal{M}_D$ of the master equation in Born-Markov approximation, and concentrating on the stationary limit one finds [28]

$$\mathcal{M}_D^I = \sum_{\nu,\nu'} \left\{S_{\nu\nu'}^{TB}(+\tau) \otimes J_\nu^T + J_\nu \otimes [S_{\nu\nu'}^{TB}(-\tau)]^T\right.$$
$$\left.-S_{\nu\nu'}^{BT}(+\tau) \otimes J_\nu^T - J_\nu \otimes [S_{\nu\nu'}^{BT}(-\tau)]^T\right\}, \tag{C3}$$

$$I_{Th} = \text{Tr}\left[\hat{I}_{Th}\rho\right] = e\sum_{ij}(\mathcal{M}_D^I)_{(j-1)\cdot 17+j,i}(\vec{\rho}_{St})_i. \tag{C4}$$

The sum over j runs over all states and stands for the trace, $1 \leq j \leq 17$, whereas the sum over i is also over all off-diagonal elements and corresponds to the matrix multiplication, thus $1 \leq i \leq 17^2 = 289$. The complicated indices of M_D^I in the sum are a result of the vectorization of the trace.

To estimate the 'leakage' current I_{Leak} mentioned in the main part of the paper we use the fact that the leakage current does not depend on the state of the Ho atom and thus can be distinguished from I_{Th}. By comparing the height of the step of the differential conductance $G = dI/dU(U)$ from elastic processes at zero bias $U = 0$ to voltages $U^> > \Delta E_{87}$ at energies above the first excitation gap, the leakage current can be estimated. The step size is defined as $s = G(U^>)/G(0) - 1$. In the experiments a step of $s_{Exp} \approx 0.9\%$ was measured. Theoretically we expect without leakage, broadening and modulation as step size of $s_{Th} \approx 10\%$. But if we assume that only 10% of the total current is described by I_{Th}, and 90% is leakage current, we would expect a step size of $s \approx 1\%$, which is in good agreement. For a more quantitative analysis of the dependence on the coupling constant c_{TB}, and thus the current, we refer to Fig. 4 c).

[1] T. Miyamachi, T. Schuh, T. Märkl, C. Bresch, T. Balashov, A. Stöhr, C. Karlewski, S. André, M. Marthaler, M. Hoffmann, M. Geilhufe, S. Ostanin, W. Hergert, I. Mertig, G. Schön, A. Ernst, and W. Wulfhekel, Nature **503**, 242 (2013).

[2] A. A. Khajetoorians, S. Lounis, B. Chilian, A. T. Costa, L. Zhou, D. L. Mills, J. Wiebe, and R. Wiesendanger, Physical Review Letters **106**, 037205 (2011).

[3] T. Balashov, T. Schuh, A. Takacs, A. Ernst, S. Ostanin, J. Henk, I. Mertig, P. Bruno,

T. Miyamachi, S. Suga, and W. Wulfhekel, Physical Review Letters **102**, 257203 (2009).

[4] S. Loth, M. Etzkorn, C. P. Lutz, D. M. Eigler, and A. J. Heinrich, Science **329**, 16281630 (2010).

[5] P. Gambardella, S. Rusponi, M. Veronese, S. S. Dhesi, C. Grazioli, A. Dallmeyer, I. Cabria, R. Zeller, P. H. Dederichs, K. Kern, C. Carbone, and H. Brune, Science **300**, 11301133 (2003).

[6] F. Donati, A. Singha, S. Stepanow, C. Wäckerlin, J. Dreiser, P. Gambardella, S. Rusponi, and H. Brune,

Physical Review Letters **113**, 237201 (2014).

[7] W. H. Zurek, Progress of Theoretical Physics **89**, 281 (1993).

[8] W. H. Zurek, Reviews of Modern Physics **75**, 715 (2003).

[9] T. Balashov, T. Miyamachi, T. Schuh, T. Märkl, C. Bresch, and W. Wulfhekel, Surface Science **630**, 331 (2014).

[10] B. Bleaney and K. W. H. Stevens, Rep. Prog. Phys. **16**, 108 (1953).

[11] R. J. Elliott and K. W. H. Stevens, Proc. Rocal Soc. A **218**, 553 (1953).

[12] B. Wybourne, *Spectroscopic properties of rare earths* (Wiley, 1965).

[13] H. J. Carmichael, *Statistical Methods in Quantum Optics 1* (Springer-Verlag Berlin Heidelberg New York, 2002).

[14] H.-P. Breuer and F. Petruccione, *The theory of open quantum systems*, 1st ed. (Oxford Univ. Press, Oxford, 2003).

[15] C. F. Hirjibehedin, C.-Y. Lin, A. F. Otte, M. Ternes, C. P. Lutz, B. A. Jones, and A. J. Heinrich, Science **317**, 1199 (2007).

[16] J. Fransson, Nano Letters **9**, 2414 (2009).

[17] C. Hübner, B. Baxevanis, A. A. Khajetoorians, and D. Pfannkuche, Phys. Rev. B **90**, 155134 (2014).

[18] F. Delgado, J. J. Palacios, and J. Fernández-Rossier, Physical Review Letters **104**, 026601 (2010).

[19] S. Loth, K. von Bergmann, M. Ternes, A. F. Otte, C. P. Lutz, and A. J. Heinrich, Nat Phys **6**, 340344 (2010).

[20] A. Donabidowicz-Kolkowska and C. Timm, New Journal of Physics **14**, 103050 (2012).

[21] W. H. Zurek, Phys. Today **67**, 44 (2014).

[22] S. Al'tshuler and B. Kozyrev, *Electron Paramagnetic Resonance in Compounds of Transition Elements* (Wiley, 1974).

[23] J. Klein, A. Leger, M. Belin, and D. Defourneau, Phys. Rev. B **7**, 2336 (1973).

[24] F. Delgado and J. Fernández-Rossier, Physical Review Letters **108**, 196602 (2012).

[25] N. Vogt, J. H. Cole, M. Marthaler, and G. Schön, Phys. Rev. B **85**, 174515 (2012).

[26] C. Karlewski and M. Marthaler, Phys. Rev. B **90**, 104302 (2014).

[27] S. Barnett, *Matrices: Methods and Applications* (Oxford University Press, 1990).

[28] J. Jin, M. Marthaler, and G. Schön, Phys. Rev. B **91**, 085421 (2015).